Optical spectroscopy of jet-cooled NiSi

Ned F. Lindholm, Dale J. Brugh, Gretchen K. Rothschopf, Shane M. Sickafoose, and Michael D. Morse[a)]
Department of Chemistry, University of Utah, Salt Lake City, Utah 84112

(Received 23 September 2002; accepted 8 November 2002)

The electronic states of gaseous diatomic NiSi have been investigated using the combined techniques of resonant two-photon ionization spectroscopy, dispersed fluorescence spectroscopy, and density functional computations. A single electronic band system, designated as the $[18.0]1 \leftarrow X\,^1\Sigma^+$ system, has been found in the 17 500–19 500 cm^{-1} range, and three bands of this system have been rotationally resolved and analyzed. To shorter wavelengths, the spectrum becomes much more congested and intense, and four bands in this region have been rotationally resolved and analyzed as well. A dispersed fluorescence investigation has allowed the measurement of 17 vibrational levels of the ground state. Through this work, the ground state of $^{58}Ni^{28}Si$ is demonstrated to have $^1\Sigma^+$ symmetry, with $r_0 = 2.0316(4)$ Å, $\omega_e = 467.43(30)$ cm^{-1}, and $\omega_e x_e = 2.046(21)$ cm^{-1}. These results are in good agreement with the results of density functional computations performed on the ground state. Comparisons to AlCu and CuSi demonstrate that NiSi has a double bond, while these related molecules are best considered as having a single σ-bond. © *2003 American Institute of Physics.* [DOI: 10.1063/1.1534107]

I. INTRODUCTION

Because of their potential use in a number of industrial applications, interest in transition metal silicides has increased greatly in the last 30 years. Like the related transition metal carbides and nitrides, transition metal silicides possess many desirable physical properties, including high melting points, low densities, and low chemical reactivity.[1] Nickel silicides in particular have demonstrated exceptional hardness and high temperature stability, and consequently their application as coatings that protect metallic surfaces against oxidation at high temperatures has been explored.[2] However, the greatest interest in nickel and other transition metal silicides is in their potential applications in the microelectronics industry. Nickel silicide has been thoroughly investigated over the past 15 years for potential applications as Schottky-barrier detectors for IR-imaging arrays,[3] contact materials for low-voltage, low-power microwave circuitry,[4] anode material in lithium batteries, and development of ULSI circuitry.[5]

Because of practical applications such as these, information concerning the fundamental chemical bonding of the gas-phase diatomic species is of interest. While several of the transition metal silicide bond energies have been measured by Knudsen effusion mass spectrometry,[6–9] considerably less information has been published concerning the gas-phase spectroscopy of these species. Cavity ringdown laser absorption spectroscopy (CRLAS) has been used by Saykally and co-workers to collect rotationally resolved spectra of CuSi,[10] AgSi,[11] AuSi,[12] and PtSi.[13] Platinum monosilicide (PtSi) has also been studied in our laboratory using resonant two-photon ionization (R2PI) spectroscopy.[14] In addition to these gas-phase spectroscopic studies, the isovalent metal silicides VSi and NbSi have been studied by ESR spectroscopy in a matrix-isolated environment.[15] For the VSi and NbSi molecules, it was found that the orbital angular momentum of the $^2\Delta_r$ ground state is quenched by interactions with the rare-gas matrix.

To our knowledge, the work reported here presents the first gas-phase spectra of NiSi. The only previous experimental work on NiSi is a determination of the dissociation energy by Knudsen effusion mass spectrometry.[6] The dissociation energy was determined to be $D_0(\mathrm{NiSi}) = 3.26 \pm 0.18$ eV using the reaction

$$\mathrm{Ni}(g) + \mathrm{Si_2C}(g) + \mathrm{C(graphite)} \rightarrow \mathrm{NiSi}(g) + \mathrm{SiC_2}(g).$$

Several theoretical investigations of NiSi have been reported.[16–18] All of these predict that the molecule has a $^1\Sigma^+$ ground state, as has been found in the isovalent NiC,[19,20] PdC,[21] PtC,[22,23] and PtSi (Refs. 13, 14) molecules.

In this paper, we present the visible spectra of jet-cooled NiSi as recorded by resonant two-photon ionization (R2PI) spectroscopy and dispersed fluorescence (DF) spectroscopy. In addition, the results of a computational investigation of the ground electronic state of the molecule using several different density functional methods are presented. The ground state is confirmed to have $^1\Sigma^+$ symmetry, and measurements of the ground- and excited state bond lengths and vibrational frequencies are provided. A discussion of the chemical bonding is given, with particular emphasis on comparisons to related molecules.

II. EXPERIMENT

The resonant two-photon spectrometer used in this work has been described previously.[24,25] The NiSi molecules are produced by laser ablation (Nd:YAG, 532 nm) of a suitable metal source (see below). The products of ablation are then swept down a 3 cm channel in a pulsed flow of helium con-

a)Electronic mail: morse@chem.utah.edu

taining 3% CH_4 (see below). The molecules are cooled to low internal temperatures by a supersonic expansion into vacuum. The molecular beam is roughly collimated by passage through a 0.5 cm diameter skimmer, and admitted into the ionization region of a reflectron time-of-flight mass spectrometer. There, the NiSi molecules are excited using a tunable Nd:YAG-pumped dye laser and subsequently ionized by a pulsed ArF excimer laser (193 nm, 6.42 eV). The molecular ions are extracted at 90° angles to the molecular beam using a Wiley–McLaren extraction assembly.[26] The molecular ions travel up a flight tube, enter a reflectron assembly,[27] and are directed down a second flight tube to a microchannel plate detector. The resulting ion signal is preamplified, digitized, and processed by a microcomputer (386 PC clone).

The optical spectra of NiSi were collected by monitoring the ion signal at masses 86 and 88 amu as a function of dye laser frequency. These masses correspond to $^{58}Ni^{28}Si$ and $^{60}Ni^{28}Si$ molecular species, which have natural abundances of 68.8% and 26.2%, respectively. Rotationally resolved spectra were recorded using an intracavity étalon inside the dye laser cavity. The dye laser was pressure scanned from 0 to 1 atm using SF_6. Reference spectra of I_2 (collected either in absorption or in fluorescence) or Te_2 (collected in absorption) were simultaneously recorded in order to determine the absolute line positions by comparison to the published reference lines of these molecules.[28–30] Measurements of unblended line positions are thought to be accurate to about 0.01 cm^{-1}.

Excited state lifetimes were measured by monitoring the ion signal as a function of delay time between the excitation and ionization lasers. The resulting decay curves are fitted to an exponential function. Excited state lifetimes are reported as the $1/e$ decay time, τ.

The spectrum of NiSi was collected using two different molecular sources. In the 22 000–25 000 cm^{-1} region, a pure Ni metal disk was first polished using SiC sandpaper, and then vaporized by laser ablation to produce the molecule of interest. In the 17 000–22 000 cm^{-1} region, a NiSi (8:1) alloy was used in place of the Ni metal disk. In both cases the inclusion of 3% CH_4 in the He carrier gas led to an increase in the NiSi ion signal, indicating that the presence of methane somehow enhances the formation of diatomic NiSi. The mechanism by which methane leads to an increase in NiSi concentration is completely unknown, and anything we might suggest would be pure speculation. Nevertheless, the inclusion of methane in the helium carrier gas causes a significant, albeit mysterious, increase in NiSi signal.

In our first experiments, using a pure Ni target disk and helium carrier gas seeded with 3% methane, our intent was to search for spectra of NiC and $NiCH_3$. The observation of spectra falling at the mass of Ni+28 initially led us to believe that $Ni \cdot C_2H_4$ was synthesized in the laser ablation plasma source. The rotationally resolved spectra were too simple for this molecule, however, and the spectra remained at the mass of Ni+28, even when the carrier gas was changed from He+3% CH_4 to He+3% CD_4. Thus, the carrier of the spectrum lacked hydrogen atoms. Eventually, we found that the same spectrum could be recorded with high intensity using pure helium carrier gas, provided the pure nickel sample was vigorously rubbed in powdered silicon prior to performing the experiment. This established the identity of the carrier of the spectrum as diatomic NiSi.

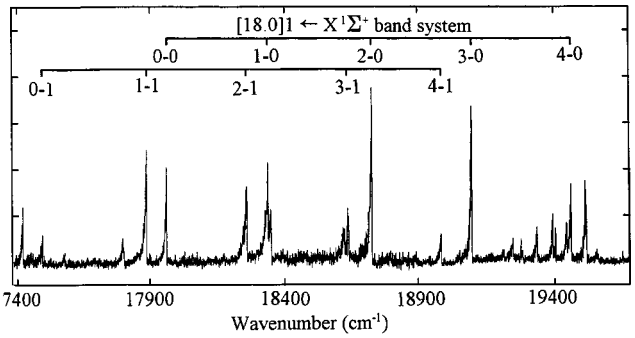

FIG. 1. Low-resolution R2PI spectrum of $^{58}Ni^{28}Si$ recorded in the range 17 400–19 700 cm^{-1}, displaying the $[18.0]1 \leftarrow X\,^1\Sigma^+$ band system of the molecule.

A detailed description of the dispersed fluorescence spectrometer has also been published.[31] Diatomic NiSi molecules were produced by focusing the fundamental radiation from a Nd:YAG laser (1064 nm) onto the Ni/Si alloy disk. The He carrier gas was once again seeded with 3% CH_4 to enhance NiSi formation. The molecular beam traveled down a 5.5 cm long channel prior to the supersonic expansion into vacuum. The supersonically cooled molecules were then irradiated by a Nd:YAG-pumped dye laser, which crossed the molecular beam at right angles approximately 1 cm downstream from the expansion orifice. The resulting fluorescence was collected at right angles to both the molecular beam and the excitation radiation, imaged onto the entrance slit of a 0.5 m spectrograph, and measured with an intensified, gated charge-coupled device. The data were collected and stored by a microcomputer for later analysis.

III. COMPUTATIONAL DETAILS

All calculations were carried out with the GAUSSIAN 98 suite of programs. Density functional calculations were performed using Becke's three-parameter hybrid functional[32] in combination with either the Lee–Yang–Parr correlation functional[33] (B3LYP), Perdew and Wang's 1991 gradient-corrected correlation functional[34–37] (B3PW91), or Perdew's 1986 nonlocal correlation expression[38](B3P86). All calculations were performed using polarized split-valence basis sets of 6-311G++(d,f) quality (++ denotes diffuse s and p functions on Si and diffuse d functions on Ni, and (d, f) denotes polarization d functions on Si and polarization f functions on Ni).

IV. RESULTS

A. The $[18.0]1 \leftarrow X^1\Sigma^+$ band system

Displayed in Fig. 1 is the low resolution spectrum of $^{58}Ni^{28}Si$, recorded over the range from 17 400 to 19 700 cm^{-1}. In this wave number range, the electronic transitions of NiSi are quite weak, but the vibronic features are sufficiently sparse for a progression to be readily identified. The weakness of the absorptions is underscored by the long fluo-

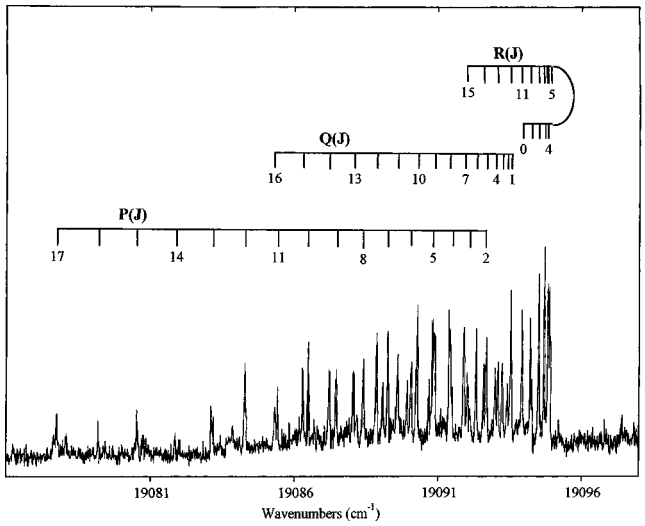

FIG. 2. Rotationally resolved scan over the 3–0 band of the $[18.0]1 \leftarrow X\,^1\Sigma^+$ system of $^{58}Ni^{28}Si$. The observation of first lines of R(0), Q(1), and P(2) confirms that this is an $\Omega' = 1 \leftarrow \Omega'' = 0$ transition.

rescence lifetimes measured, which lie in the range of 7–8 μs. Despite the low density of vibronic features, perturbations are clearly evident in the split features found for the 1–0 and 4–0 bands.

Rotationally resolved studies were successfully undertaken for the bands near 18 719, 19 094, and 19 456 cm^{-1}, which are labeled in Fig. 1 as the 2–0, 3–0, and 4–0 bands, respectively. The rotationally resolved spectrum of the 19 094 cm^{-1} band, which is similar to that recorded for the other two bands, is displayed in Fig. 2 for the dominant isotopomer, $^{58}Ni^{28}Si$. As was found for bands investigated in almost exactly the same wavelength region for the isovalent PtSi molecule, the spectrum exhibits a head in the R branch, along with a Q and a P branch. The first lines in the respective branches are R(0), Q(1), and P(2), demonstrating that the transition occurs between Hund's case (a) states that are characterized by $\Omega' = 1$ and $\Omega'' = 0$.

Assuming that the ground state is indeed the theoretically predicted $^1\Sigma^+$ state, which is consistent with our measured value of $\Omega'' = 0$, the rotationally resolved spectra of the 2–0, 3–0, and 4–0 bands were fitted to the expression[39]

$$\nu = \nu_0 + B'J'(J'+1) \pm (q'/2)J'(J'+1) - B''J''(J''+1), \tag{4.1}$$

which is valid for a $^1\Pi \leftarrow X\,^1\Sigma^+$ transition. Here, the $\pm$ sign refers to the e/f levels, respectively, of the $^1\Pi$ upper state, and the parameter q' accounts for the lambda doubling that is associated with this state. As the $X\,^1\Sigma^+$ ground state has e levels only, the P and R branches terminate on e levels of the upper state, and are fitted using the $+$ sign in Eq. (4.1). The Q branch, on the other hand, terminates on f levels and is therefore fitted using the $-$ sign in Eq. (4.1).

The measured rotational line positions for all rotationally resolved bands were simultaneously fitted to extract the most accurate values of the spectroscopic constants. A complete listing of the fitted rotational lines, along with fitted spectroscopic constants for all of the rotationally resolved bands of $^{58}Ni^{28}Si$ and $^{60}Ni^{28}Si$, is available via the Electronic Physics Auxiliary Publication Service (EPAPS) or through the author (M.D.M.).[40] The results of these rotational fits are included in Table I.

Although the bands listed in Table I and displayed in Fig. 1 clearly form a band system, the vibrational numbering of the bands remains to be determined. For many molecules this may be established by examining the isotope shifts of the observed bands. For a band system that may be fitted to the simple anharmonic oscillator expression

$$\nu = T_0 + \omega_e' v' - \omega_e' x_e' (v'^2 + v') - \omega_e'' v'' + \omega_e'' x_e'' (v''^2 + v''), \tag{4.2}$$

TABLE I. Measured spectroscopic properties of NiSi. Quantities in parentheses represent the 1σ error limits, in units of the last reported digits.

Band system	Band $v'-v''$	$\Omega' \leftarrow \Omega''$	$^{58}Ni^{28}Si$		$^{60}Ni^{28}Si$		$\Delta\nu$ (cm^{-1})	τ (μs)
			ν_0 (cm^{-1})	B' (cm^{-1})	ν_0 (cm^{-1})	B' (cm^{-1})		
$[18.0]1 \leftarrow X\,^1\Sigma^+$	0–1	$1 \leftarrow 0^+$	17 489[a]		17 490[a]		−0.7[a]	
	0–0	$1 \leftarrow 0^+$	17 956[a]		17 954[a]		1.5[a]	
	2–1	$1 \leftarrow 0^+$	18 257[a]		18 255[a]		1.6[a]	
	1–0	$1 \leftarrow 0^+$	18 334 or 18 345[b]		18 336[a]		⋯	
	3–1	$1 \leftarrow 0^+$	18 617 or 18 633[b]		18 620[a]		⋯	
	2–0	$1 \leftarrow 0^+$	18 719.4326(25)	0.189 162(57)[c]	18 714.7301(26)	0.186 087(90)[c]	4.7025(36)	7.
	4–1	$1 \leftarrow 0^+$	18 982[a]		18 975[a]		7.1[a]	
	3–0	$1 \leftarrow 0^+$	19 093.5955(27)	0.185 629(53)[c]	19 086.7659(52)	0.182 089(84)[c]	6.8296(59)	8.
	4–0	$1 \leftarrow 0^+$	19 455.7769(25)	0.175 354(60)[c]	19 448.7163(29)	0.176 255(132)[c]	7.0606(38)	
Unclassified bands		$0^+ \leftarrow 0^+$	22 857.9101(23)	0.161 538(87)	22 852.6819(20)	0.160 262(90)	5.2282(30)	0.18
		$0^+ \leftarrow 0^+$	22 973.3156(41)	0.160 354(73)	22 966.9268(43)	0.151 311(158)	6.3888(59)	0.20
		$0^+ \leftarrow 0^+$	23 084.7157(35)	0.158 400(66)	23 078.9005(38)	0.157 831(113)	5.8152(52)	0.34
		$0^+ \leftarrow 0^+$	23 306.7016(19)	0.157 675(55)	23 299.4540(27)	0.155 267(68)	7.2476(33)	0.17

[a]Measured in low resolution, with imperfect calibration. The measurement is expected to be accurate to ± 5 cm^{-1}. Isotope shift measurements are less affected by poor calibration, and are thought to be accurate to about 0.5 cm^{-1}.

[b]Overlapped or perturbed feature, preventing an estimate of the isotope shift.

[c]Lambda doubling in the $\Omega' = 1$ upper state is described by the parameter q', as described in the text. Fitted values of this parameter for the $v' = 2$, 3, and 4 levels of $^{58}Ni^{28}Si$ are: 0.001 700(40), 0.000 819(28), and −0.000 545(35) cm^{-1}, respectively. The corresponding values for $^{60}Ni^{28}Si$ are: −0.000 778(91), 0.001 238(148), and 0.000 741(43) cm^{-1}.

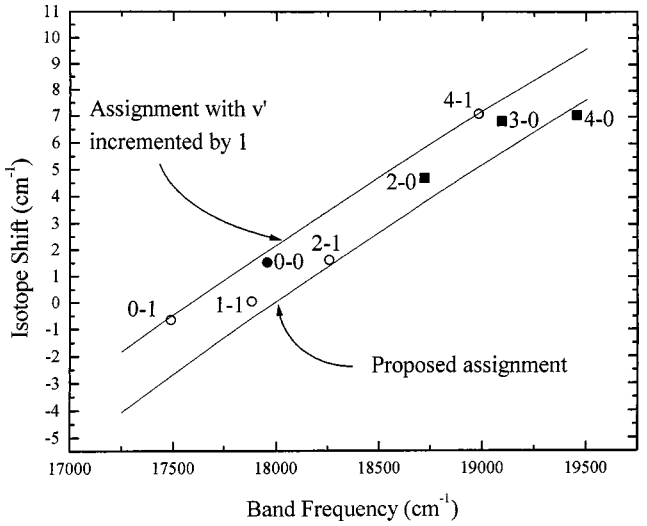

FIG. 3. Measured and calculated isotope shifts of the $[18.0]1 \leftarrow X\,^1\Sigma^+$ band system. Isotope shifts precisely measured in high resolution are shown with filled squares; filled circles provide low resolution measurements of isotope shifts for bands originating from $v''=0$; open circles are for low resolution measurements for bands originating from $v''=1$. See the text for details.

the isotope shift is given by

$$\Delta\nu \equiv \nu(^{58}\mathrm{Ni}^{28}\mathrm{Si}) - \nu(^{60}\mathrm{Ni}^{28}\mathrm{Si}) = (1-\rho)\omega_e' v' + \tfrac{1}{2}(1-\rho)(\omega_e' - \omega_e'') - (1-\rho^2) \times \omega_e' x_e' (v' + \tfrac{1}{2})^2 + \tfrac{1}{4}(1-\rho^2)\omega_e'' x_e'', \quad (4.3)$$

for $v''=0$, with ρ defined as

$$\rho \equiv \sqrt{\frac{\mu(^{58}\mathrm{Ni}^{28}\mathrm{Si})}{\mu(^{60}\mathrm{Ni}^{28}\mathrm{Si})}}. \quad (4.4)$$

Equations (4.2)–(4.4) may therefore be used to calculate the expected isotope shift for a given assignment of the observed vibrational bands, and this may be compared to the measured isotope shifts. Such a comparison is displayed in Fig. 3, where the measured isotope shifts are presented as filled squares (for shifts measured in high resolution), filled circles (for bands originating from $v''=0$, measured in low resolution), and open circles (for bands originating from $v''=1$, measured in low resolution). The solid lines represent the calculated isotope shifts obtained using Eq. (4.3) for two different vibrational numberings: one in which the 17 956 cm^{-1} band is assigned as the 0–0 band (proposed assignment) and another in which it is assigned as the 1–0 band. The reliably measured isotope shifts of the 18 719 and 19 093 cm^{-1} bands fall between these two choices, while the isotope shift of the perturbed 19 456 cm^{-1} band lies near the line that is based on our proposed assignment. The isotope shifts measured in low resolution clearly support the assignment of these features to a common electronic band system, but they are of little help in establishing the vibrational numbering. Either vibrational numbering could be correct, but the lack of a 0–0 band in the spectrum under the latter assignment suggests that this assignment is incorrect. On this basis, the vibrational numbering given in Fig. 1 and Table I is adopted.

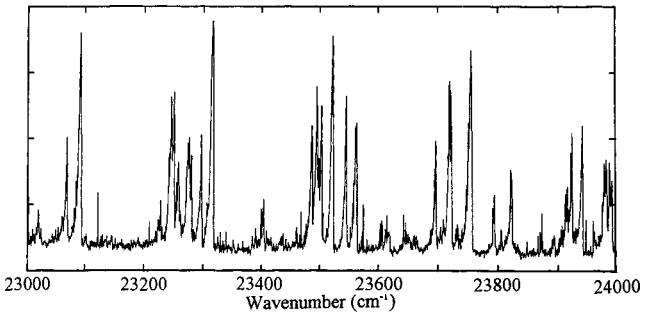

FIG. 4. Low resolution R2PI spectrum of $^{58}\mathrm{Ni}^{28}\mathrm{Si}$, recorded in the higher wave number range 23 000–24 000 cm^{-1}. Here, the spectrum is very congested and much more intense than in the lower frequency region.

The bands assigned to the $[18.0]1 \leftarrow X\,^1\Sigma^+$ band system in Table I were fitted to extract vibrational constants ω_e' and $\omega_e' x_e'$, and the fitted B_v' values were used to extract the rotational constants B_e', α_e', and r_e'. These are reported in Table II, along with spectroscopic constants for the $X\,^1\Sigma^+$ ground state. Because of the perturbation in the $v'=4$ level of the $^{58}\mathrm{Ni}^{28}\mathrm{Si}$ isotope, the r_e' value obtained from the $^{60}\mathrm{Ni}^{28}\mathrm{Si}$ species is felt to more accurately represent the [18.0]1 state of this molecule.

B. The spectrum of NiSi in the 22 700–26 300 cm^{-1} region

To higher wave numbers, the spectrum of NiSi becomes much more congested and considerably more intense, as is illustrated in Fig. 4. Despite numerous attempts, we have failed to identify vibronic progressions or electronic band systems among these transitions. Perturbations between

TABLE II. Electronic states of $^{58}\mathrm{Ni}^{28}\mathrm{Si}$ and $^{60}\mathrm{Ni}^{28}\mathrm{Si}$. Fitted parameters are provided, with 1σ error limits given in parentheses in units of the last digits quoted. Although the measured values of B_0'' and r_0'' seem fantastically precise, the fact that the values of r_0'' for $^{58}\mathrm{Ni}^{28}\mathrm{Si}$ and $^{60}\mathrm{Ni}^{28}\mathrm{Si}$ agree to within their 1σ error limits suggests that the error limits are correct.

Molecule	State	T_0 (cm^{-1})	ω_e (cm^{-1})	$\omega_e x_e$ (cm^{-1})	B_e (cm^{-1})	α_e (cm^{-1})	r_e (Å)	τ (μs)
$^{58}\mathrm{Ni}^{28}\mathrm{Si}$	[18.0]1	17 956.5(2.8)	396.5(3.6)	4.47(70)	0.207 55(789)	0.0069(41)	2.075(39)	7.5
	$X\,^1\Sigma^+$	0.0000	467.43(30)[a]	2.046(21)[a]	$B_0''=0.216\,476(51)$		$r_0''=2.031\,65(24)$	⋯
$^{60}\mathrm{Ni}^{28}\mathrm{Si}$	[18.0]1	17 953.8(2.8)	394.4(3.7)	4.33(73)	0.198 68(215)	0.0049(11)	2.109(11)	7.5
	$X\,^1\Sigma^+$	0.0000	464.89(30)[a]	2.024(21)[a]	$B_0''=0.214\,144(84)$		$r_0''=2.031\,58(40)$	⋯

[a]The fitted values of ω_e'' and $\omega_e'' x_e''$ for the $X\,^1\Sigma^+$ ground state are obtained from dispersed fluorescence measurements, where the excitation frequency was optimized to give the strongest fluorescence signal. Accordingly, it is thought that this corresponds to the excitation of the dominant isotopomer, $^{58}\mathrm{Ni}^{28}\mathrm{Si}$. The values of ω_e'' and $\omega_e'' x_e''$ for $^{60}\mathrm{Ni}^{28}\mathrm{Si}$ are calculated from those of $^{58}\mathrm{Ni}^{28}\mathrm{Si}$ by correcting for the differences in reduced mass between the two species.

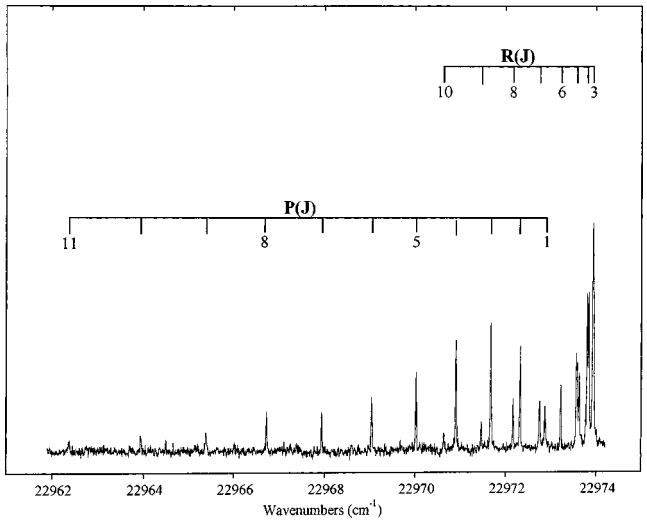

FIG. 5. Rotationally resolved spectrum of a band of $^{58}Ni^{28}Si$ near 22 973 cm^{-1}. This is typical of the $\Omega' = 0 \leftarrow \Omega'' = 0$ bands found in the higher wave number range displayed in Fig. 4.

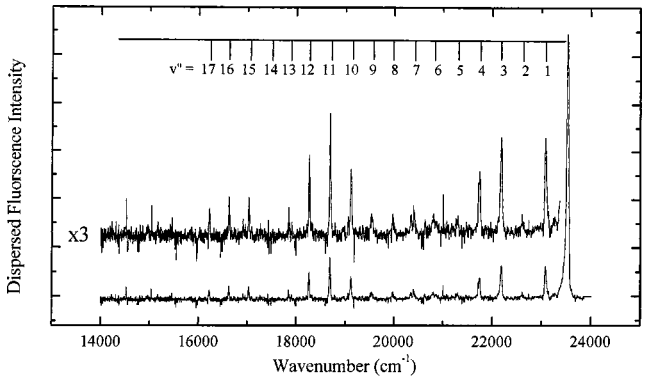

FIG. 6. Dispersed fluorescence spectrum obtained by excitation of a band of $^{58}Ni^{28}Si$ near 23 544 cm^{-1}. Because of the large change in bond length upon electronic excitation, fluorescence to a long progression of vibrational levels of the ground state is observed.

states in this energy region are rampant, making the identification of electronic band systems an exercise in futility. Nevertheless, we have successfully rotationally resolved and analyzed four of the vibronic bands in the 22 850–23 310 cm^{-1} range. All of the resolved bands are $\Omega' = 0 \leftarrow \Omega'' = 0$ transitions, lacking a Q branch, and all have a head quite early in the R branch. These were fitted using a formula similar to that of Eq. (4.1), with the lambda-doubling term involving q' dropped. A typical example is shown in Fig. 5, which displays the rotationally resolved band of $^{58}Ni^{28}Si$ near 22 973 cm^{-1}. The results of rotational fits of these bands are provided in Table I.

While the lower frequency region is dominated by a weak $\Omega' = 1 \leftarrow X\,^1\Sigma^+$ band system, the higher frequency region is apparently dominated by parallel transitions. Based on the $X\,^1\Sigma^+$ symmetry of the ground state, these are $\Omega' = 0^+ \leftarrow \Omega'' = 0^+$ in character. It appears that a $^1\Sigma^+$ state with a large electric dipole matrix element connecting it to the ground state lies in this energy range, and vibronic or spin–orbit interactions couple this state to other states with $\Omega' = 0^+$. This leads to a large number of vibronically mixed states that exhibit electric-dipole allowed transitions with the ground state. Remnants of the $^1\Sigma^+$ state that provides the source of the oscillator strength may perhaps be discerned in Fig. 4, where the spectrum is observed to display clumps of intensity spaced roughly 210 cm^{-1} apart. This suggests a vibrational frequency of roughly 210 cm^{-1} for the $^1\Sigma^+$ state that provides the source of oscillator strength in this spectral region.

C. Measurement of ground-state vibrational constants

The ground-state vibrational frequency of NiSi was determined by excitation of 11 transitions in the 22 800–24 400 cm^{-1} range and recording the dispersed fluorescence (DF) spectrum of each. As an example, the DF spectrum obtained by exciting a band at 23 544 cm^{-1} is presented in Fig. 6. While previous theoretical investigations predict the presence of many low-lying electronic states,[16,17] fluorescence was only observed to the vibrational levels of the ground state. The dispersed fluorescence data obtained from all 11 excitations were combined and fitted to the standard expression for an anharmonic oscillator

$$G''(v'') - G''(0) = \omega_e'' v'' - \omega_e'' x_e'' (v''^2 + v''), \tag{4.5}$$

to obtain values of the spectroscopic parameters ω_e'' and $\omega_e'' x_e''$. Because of the large change in bond length upon electronic excitation, 17 vibrational levels of the ground state were observed in the dispersed fluorescence spectra, allowing the vibrational constants of the ground state to be rather well determined. Further, because the excitation wavelength was optimized to provide the highest intensity in the fluorescence signal, we believe that the fluorescence arises from the most abundant isotopomer, $^{58}Ni^{28}Si$ (63%). Accordingly, the measured vibrational constants pertain to this species. The values listed in Table II for $^{60}Ni^{28}Si$ are derived from those measured for $^{58}Ni^{28}Si$ using the well-known dependence of ω_e and $\omega_e x_e$ on the reduced mass

$$\omega_e(^{60}Ni^{28}Si) = \sqrt{\frac{\mu(^{58}Ni^{28}Si)}{\mu(^{60}Ni^{28}Si)}}\,\omega_e(^{58}Ni^{28}Si), \tag{4.6}$$

and

$$\omega_e x_e(^{60}Ni^{28}Si) = \frac{\mu(^{58}Ni^{28}Si)}{\mu(^{60}Ni^{28}Si)}\,\omega_e x_e(^{58}Ni^{28}Si). \tag{4.7}$$

D. Comparison to density functional calculations

Table III presents the results of our theoretical investigation of the ground electronic state of diatomic NiSi, along with previous studies. In the present investigation, three different density functional methods were used to calculate the bond length, vibrational frequency, and bond energy of the ground state. All three methods obtained a bond length within 1% of the spectroscopic measurement, yielding a marked improvement over previous calculations. While the density functional calculation of the bond length of NiSi performed by Andriotis and co-workers[18] does fall closer to the measured value than either of the previous variational stud-

TABLE III. Calculated molecular constants of the $X\,^1\Sigma^+$ ground state of $^{58}Ni^{28}Si$.

Level of theory	r_e (Å)	D_e (eV)	ω_e (cm^{-1})	Dipole moment (debye)
MRDCI[a]	2.24	1.89	303	0.677
HF-CI[b]	2.23	1.13	313	⋯
CASSCF[c]	2.14	1.28(2.35)	416	⋯
B3LYP DFT[d]	2.142	⋯	400	⋯
B3LYP DFT[e]	2.016	2.35	499.69	0.631
B3PW91[e]	2.010	2.32	507.26	0.933
B3P86[e]	2.004	2.49	512.21	0.812
Experiment	$r_0=2.032$[e]	3.26 ± 0.18[f]	467.43(30)[e]	⋯

[a]Reference 16.
[b]Reference 17.
[c]Reference 17. When the calculated error between the $3d^84s^2$ and $3d^94s^1$ states of atomic nickel is accounted for, the calculated value of the bond dissociation energy, D_e, changes from 1.28 to 2.35 eV. Contrary to the statement made in Ref. 17, this is still substantially less than the value of $D_0=3.26\pm0.18$ eV reported in Ref. 6.
[d]Reference 18, performed using the 6-311G* basis set.
[e]This work.
[f]Reference 6.

ies, the density functional results obtained in the present study are in much better agreement with experiment than any of the previous theoretical results. This is probably a result of the additional polarization and diffuse functions used in the present study. In calculating the properties of related molecules, such as FeSi and CoSi, using the density functional method, it will obviously be important to include these additional functions in the basis set. While each of the three DFT calculations reported here overestimates the vibrational frequency by a significant amount, the present calculations still provide a substantial improvement over previous studies.

The least accurately calculated property is the bond energy. All three DFT methods employed in the present study underestimate the bond energy by 0.8 eV or more. Given the good agreement found for the bond length and the slight overestimate of the vibrational frequency found with these methods, such a large underestimate for the bond energy is a bit surprising. One could imagine that a systematic error in the Knudsen effusion measurement might be at work, and that the true bond energy might lie closer to the DFT values calculated here. To test this hypothesis, we have calculated the bond energy based on the assumption that the ground state follows the Morse potential formula

$$G(v)=\omega_e(v+\tfrac{1}{2})-\omega_e x_e(v+\tfrac{1}{2})^2, \tag{4.8}$$

all the way out to the dissociation limit. With this assumption, the bond energy, $D_e(\mathrm{NiSi})$, is given by

$$D_e(\mathrm{NiSi})=\frac{\omega_e^2}{4\omega_e x_e}. \tag{4.9}$$

The values of ω_e and $\omega_e x_e$ reported in Table II then lead to an estimate of $D_e(\mathrm{NiSi})=3.31$ eV, in excellent agreement with the Knudsen effusion result of 3.26 ± 0.18 eV.[6] Using Eq. (4.9) with the vibrational parameters of the [18.0]1 state leads to a bond energy of the [18.0]1 state of 1.09 eV. Adding this value to the term energy of the [18.0]1 state predicts a dissociation limit lying 3.32 eV above the molecular ground state. Again, this is in excellent agreement with the Knudsen effusion value.[6] The agreement of both of these Morse potential values with the Knudsen effusion result validates the Knudsen diffusion measurement, and suggests that both the $X\,^1\Sigma^+$ ground state and the [18.0]1 state dissociate to the same separated atom limit. In fact, this latter point need not be true, because the Ni $3d^94s^1$, ^3D and $3d^84s^2$, ^3F states are nearly degenerate, and the [18.0]1 state could dissociate to either of these limits based on our data.

V. DISCUSSION

In thinking about the electronic structure of diatomic NiSi, one must begin with the molecular orbitals that are responsible for the chemical bond. *Ab initio* studies of NiSi (Refs. 16, 17) assert that the chemical bond arises from Si in its $^3P(3s^2\,3p^2)$ ground state, and Ni in its $^3D(3d^9\,4s^1)$ state. This results in a doubly occupied σ-bonding molecular orbital formed by overlap of the singly occupied $4s_{\mathrm{Ni}}$ and $3p\sigma_{\mathrm{Si}}$ orbitals, along with a π bond formed by the valence bond coupling of a $3d\pi_{\mathrm{Ni}}$ electron with a $3p\pi_{\mathrm{Si}}$ electron.[17] Along with the $3s$ orbital of Si, these form the low-lying 9σ, 10σ, and 4π orbitals, with the 9σ orbital being largely Si $3s$ in character. Above these orbitals lie the nonbonding 1δ and 11σ orbitals, which are predominantly $3d_{\mathrm{Ni}}$ in character, and the antibonding 5π and 12σ orbitals.[17] Calculations indicate that the ground state of NiSi is a combination of the $9\sigma^2\,10\sigma^2\,4\pi^4\,1\delta^4\,11\sigma^2$, $^1\Sigma^+$ and $9\sigma^2\,10\sigma^2\,4\pi^3\,1\delta^4\,11\sigma^2\,5\pi^1$, $^1\Sigma^+$ configurations, with significant contributions from other configurations as well.[17] The multiconfigurational nature of this system presumably arises from the valence bond coupling of the $3d\pi_{\mathrm{Ni}}$ and $3p\pi_{\mathrm{Si}}$ systems, which cannot be represented in a single molecular orbital configuration. Rotationally resolved spectra recorded in this study have shown NiSi to have $\Omega''=0$ in its ground state, which is consistent with the $^1\Sigma^+$ ground state predicted by theory. With the electronic ground states of the isovalent molecules NiC,[19,20] PdC,[21] PtC,[22,23] and PtSi (Refs. 13, 14) known to be $^1\Sigma^+$ as well, there is no reason to expect a different ground state for NiSi.

The bond length of NiSi [$r_0''=2.0316(4)$ Å] reported in this work is much shorter than the bond length of its isoelectronic counterpart AlCu [$r_0''=2.3389(4)$ Å].[41] Similarly, the bond energy of NiSi ($D_0''=3.26\pm0.18$ eV) (Ref. 6) is much greater than that of AlCu (2.315 ± 0.012 eV).[41] These differences are reflected in the vibrational frequencies, which are measured as 467.43 cm^{-1} for NiSi (ω_e'') and 293 cm^{-1} for AlCu ($\Delta G_{1/2}$).[41] These comparisons demonstrate that the chemical bonding differs significantly between the two species. While both molecules possess a strong σ bond, the possibility of π bonding is favorable only in NiSi. The AlCu molecule could, in principle, form a π bond by donation of a $d\pi$ electron pair from the more electronegative Cu atom into the empty $3p\pi$ orbital of the electropositive Al atom. This situation is highly unfavorable, however, because the electronegativity difference goes the wrong way. Although a small amount of delocalization of the Cu $d\pi$ electrons likely occurs, the unfavorable electronegativities of the atoms suppresses this π-bonding interaction. Thus, it is fair to classify

AlCu as having a single bond while NiSi has a double bond.

Diatomic CuSi has also been studied, using both theoretical calculations[42–45] and spectroscopic measurements.[10] While possessing only one more electron than NiSi, CuSi lacks the π bond that is present in NiSi. This occurs because the Cu atom has a full $3d$ subshell, causing these orbitals to be more severely contracted and to lie lower in energy than in nickel. As a result, the $3d$ subshell is more corelike in Cu. While CuSi does possess a strong σ bond, the corelike behavior of the $3d$ electrons strongly hinders any π-bonding interactions. This also leaves the $3p\pi_{\mathrm{Si}}$ electron unpaired in the 5π orbital, which is nonbonding or perhaps slightly antibonding in character. By comparing the bond energies of CuSi (2.36 ± 0.16 eV) (Ref. 46) and NiSi (3.26 ± 0.18 eV),[6] as determined by Knudsen effusion mass spectroscopy, it may be noted that CuSi is much more similar in its bonding to AlCu (2.315 ± 0.012 eV) (Ref. 41) than to NiSi. This confirms the lack of significant π bonding in CuSi.

VI. CONCLUSION

Electronic spectra of jet-cooled NiSi have been recorded using resonant two-photon ionization and dispersed fluorescence spectroscopies. Rotationally resolved R2PI studies have determined the ground state to be of $^1\Sigma^+$ symmetry, with a bond length of $r_0''=2.0316(4)$ Å. Dispersed fluorescence measurements of the ground-state vibrational levels have been analyzed to provide $\omega_e''=467.43(30)$ cm^{-1} and $\omega_e x_e''=2.05(2)$ cm^{-1}. Comparison to the isoelectronic AlCu and to the related CuSi molecules demonstrates the importance of π bonding in NiSi. While AlCu and CuSi are best considered as having only a σ bond, NiSi has a π bond in addition to the σ bond.

ACKNOWLEDGMENTS

This material is based upon work supported by the National Science Foundation under Grant No. 0078993. We would also like to thank Professor Tim Steimle for his gift of isotopically pure ^{130}Te in a sealed absorption cell, which was used to calibrate the rotationally resolved spectra collected from 20 000 to 23 000 cm^{-1}.

[1] *Silicon Chemistry*, edited by E. R. Corey, J. Y. Corey, and P. P. Gaspar (Ellis Harwood, Chichester, UK, 1988).
[2] X. B. Liu, L. G. Yu, and H. M. Wang, J. Mater. Sci. Lett. **20**, 1489 (2001).
[3] J. Kurianski, J. Van Damme, J. Vermeiren, K. Maex, and C. Claeys, Proc. SPIE-Int. Soc. Opt. Eng. **1308**, 27 (1990).
[4] J. Chen, J. P. Colinge, D. Flandre, R. Gillon, J. P. Raskin, and D. Vanhoenacker, J. Electrochem. Soc. **144**, 2437 (1997).
[5] D. X. Xu, S. R. Das, C. J. Peters, and L. E. Erickson, Thin Solid Films **326**, 143 (1998).
[6] A. V. Auwera-Mahieu, N. S. McIntyre, and J. Drowart, Chem. Phys. Lett. **4**, 198 (1969).
[7] A. V. Auwera-Mahieu, R. Peeters, N. S. McIntyre, and J. Drowart, Trans. Faraday Soc. **66**, 809 (1970).
[8] K. A. Gingerich, R. Haque, and J. E. Kingcade, Jr., Thermochim. Acta **30**, 61 (1979).
[9] I. Shim and K. A. Gingerich, Z. Phys. D: At., Mol. Clusters **12**, 373 (1989).
[10] J. J. Scherer, J. B. Paul, C. P. Collier, and R. J. Saykally, J. Chem. Phys. **102**, 5190 (1995).
[11] J. J. Scherer, J. B. Paul, C. P. Collier, and R. J. Saykally, J. Chem. Phys. **103**, 113 (1995).
[12] J. J. Scherer, J. B. Paul, C. P. Collier, A. O'Keefe, and R. J. Saykally, J. Chem. Phys. **103**, 9187 (1995).
[13] J. B. Paul, J. J. Scherer, C. P. Collier, and R. J. Saykally, J. Chem. Phys. **104**, 2782 (1996).
[14] L. Shao, S. M. Sickafoose, J. D. Langenberg, D. J. Brugh, and M. D. Morse, J. Chem. Phys. **112**, 4118 (2000).
[15] Y. M. Hamrick and W. Weltner, Jr., J. Chem. Phys. **94**, 3371 (1991).
[16] H. Haberlandt, Chem. Phys. **138**, 315 (1989).
[17] I. Shim and K. A. Gingerich, Z. Phys. D: At., Mol. Clusters **16**, 141 (1990).
[18] A. N. Andriotis, M. Menon, G. E. Froudakis, Z. Fthenakis, and J. E. Lowther, Chem. Phys. Lett. **292**, 487 (1998).
[19] M. A. Brewster and L. M. Ziurys, Astrophys. J. **559**, 1190 (2001).
[20] D. J. Brugh and M. D. Morse, J. Chem. Phys. **117**, 10703 (2002).
[21] J. D. Langenberg, L. Shao, and M. D. Morse, J. Chem. Phys. **111**, 4077 (1999).
[22] T. C. Steimle, K. Y. Jung, and B.-Z. Li, J. Chem. Phys. **102**, 5937 (1995).
[23] S. A. Beaton and T. C. Steimle, J. Chem. Phys. **111**, 10876 (1999).
[24] Z. Fu, G. W. Lemire, Y. M. Hamrick, S. Taylor, J.-C. Shui, and M. D. Morse, J. Chem. Phys. **88**, 3524 (1988).
[25] G. W. Lemire, G. A. Bishea, S. A. Heidecke, and M. D. Morse, J. Chem. Phys. **92**, 121 (1990).
[26] W. C. Wiley and I. H. McLaren, Rev. Sci. Instrum. **26**, 1150 (1955).
[27] B. A. Mamyrin, V. I. Karataev, D. V. Shmikk, and V. A. Zagulin, Zh. Éksp. Teor. Fiz. **64**, 82 (1973).
[28] S. Gerstenkorn and P. Luc, *Atlas du Spectre d'Absorption de la Molécule d'Iode entre 14 800–20 000 cm^{-1}* (CNRS, Paris, 1978).
[29] S. Gerstenkorn and P. Luc, Rev. Phys. Appl. **14**, 791 (1979).
[30] J. Cariou and P. Luc, *Atlas du Spectre d'Absorption de la Molécule de Tellure entre 18 500–23 800 cm^{-1}* (CNRS, Paris, 1980).
[31] R. S. DaBell, R. G. Meyer, and M. D. Morse, J. Chem. Phys. **114**, 2938 (2001).
[32] A. D. Becke, J. Chem. Phys. **98**, 5648 (1993).
[33] C. Lee, W. Yang, and R. G. Parr, Phys. Rev. B **37**, 785 (1988).
[34] K. Burke, J. P. Perdew, and Y. Wang, *Electronic Density Functional Theory: Recent Progress and New Directions* [Proceedings of the International Workshop on Electronic Density Functional Theory: Recent Progress and New Directions], Nathan, Australia, 14–19 July, 1996, 81–111 (1998).
[35] J. P. Perdew, J. A. Chevary, S. H. Vosko, K. A. Jackson, M. R. Pederson, D. J. Singh, and C. Fiolhais, Phys. Rev. B **46**, 6671 (1992).
[36] J. P. Perdew, J. A. Chevary, S. H. Vosko, K. A. Jackson, M. R. Pederson, D. J. Singh, and C. Fiolhais, Phys. Rev. B **48**, 4978 (1993).
[37] J. P. Perdew, K. Burke, and Y. Wang, Phys. Rev. B **54**, 16533 (1996).
[38] J. P. Perdew and W. Yue, Phys. Rev. B **33**, 8800 (1986).
[39] J. M. Brown and A. J. Merer, J. Mol. Spectrosc. **74**, 488 (1979).
[40] See EPAPS Document No. E-JCPSA6-118-025305 for 10 pages of absolute line positions and rotational fits. This document may be retrieved via the EPAPS homepage (http://www.aip.org/pubservs/epaps.html) or from ftp.aip.org in the directory /epaps/. See the EPAPS homepage for more information.
[41] J. M. Behm, C. A. Arrington, J. D. Langenberg, and M. D. Morse, J. Chem. Phys. **99**, 6394 (1993).
[42] A. I. Boldyrev, J. Simons, J. J. Scherer, J. B. Paul, C. P. Collier, and R. J. Saykally, J. Chem. Phys. **108**, 5728 (1998).
[43] P. Turski and M. Barysz, J. Chem. Phys. **111**, 2973 (1999).
[44] P. Turski, Chem. Phys. Lett. **315**, 115 (1999).
[45] P. Turski and M. Barysz, J. Chem. Phys. **113**, 4654 (2000).
[46] G. Riekert, P. Lamparter, and S. Steeb, Z. Metallkd. **72**, 765 (1981).